Testing viable $f(R)$ models with the angular-diameter distance to compact quasar cores

Joseph Sultana*
Department of Mathematics, Faculty of Science, University of Malta, Msida MSD2080, Malta

Fulvio Melia†
Department of Physics, The Applied Math Program, and Department of Astronomy, The University of Arizona, Tucson Arizona 85721, USA

Demosthenes Kazanas‡
Astrophysics Science Division, NASA/Goddard Space Flight Center, Greenbelt, Maryland 20771, USA

(Received 24 November 2018; published 6 May 2019)

We consider here some popular $f(R)$ models generally viewed as possible alternatives to the existence of dark energy in General Relativity. For each of these, we compute the redshift $z_{\max}$ at which the angular diameter distance $d_A(z)$ is expected to reach its maximum value. This turning point in $d_A(z)$ was recently measured in a model-independent way using compact quasar cores and was found to occur at $z_{\max} = 1.70 \pm 0.20$. We compare the predictions of $z_{\max}$ for the $f(R)$ models with this observed value to test their viability at a deeper level than has been attempted thus far, thereby quantifying an important observational difference between such modified gravity scenarios and standard Lambda Cold Dark Matter (ΛCDM) cosmology. Our results show that, while the most popular $f(R)$ models today are consistent with this measurement to within 1σ, the turning point $z_{\max}$ will allow us to prioritize these alternative gravity theories as the measurement precision continues to improve, particularly with regard to how well they mitigate the tension between the predictions of ΛCDM and the observations. For example, while the Hu-Sawicki version of $f(R)$ increases this tension, the Starobinky model reduces it.

DOI: 10.1103/PhysRevD.99.103505

I. INTRODUCTION

During the last two decades there has been a renewed interest in the modification of Einstein's General Relativity theory, mainly in the field of cosmology, in a bid to obtain a more fundamental explanation for the accelerated expansion of the Universe during its inflationary and dark energy epochs. In these modified theories, the repulsive force driving the accelerated expansion arises as a purely geometric effect [1]. In this way, one tries to evade the coincidence and cosmological problems of standard Lambda Cold Dark Matter (ΛCDM) cosmology in General Relativity (GR) or the origin of some yet-to-be-observed scalar field in the so-called scalar-tensor cosmological models [2]. In these modified theories, the Einstein-Hilbert Lagrangian is altered by replacing the Ricci scalar R with a nonlinear function, containing other curvature invariants, such as $f(R, R_{ab}R^{ab}, R_{abcd}R^{abcd}, \ldots)$. One of the simplest and most natural extensions of GR in this class is known as $f(R)$ gravity [3], a prominent and well-studied theory. Other extensions include Gauss-Bonnet gravity [4,5], Finsler-Randers gravity [6], and conformal Weyl gravity [7].

Following Starobinsky's inflationary model [8] of the early Universe with $f(R) = R + \alpha R^2$ and the first attempt [9] to mimic the late time cosmic acceleration with $1/R$ gravity—a model that was later ruled out due to its instabilities [10,11] and violation of the post-Newtonian tests of GR [12]—the theory of $f(R)$ gravity has been studied extensively, with numerous $f(R)$ models being proposed over the past decade. Some of these are attractive because they can apparently describe the early phase of inflation as well as the current accelerated expansion of the Universe [13]. Many others fail to predict a matter-dominated era [14,15] in the expansion history of the Universe, however, and therefore cannot be considered as viable $f(R)$-gravity models. Thus far, only a few observationally viable $f(R)$ models also satisfy the Solar System tests. Some popular examples include the models found in Refs. [16–19].

In some cases, it was originally claimed that these $f(R)$ models do not contain a cosmological constant Λ. It can

*joseph.sultana@um.edu.mt
†fmelia@email.arizona.edu
‡Demos.Kazanas-1@nasa.gov

easily be shown [20], however, that all these cosmologies do in fact contain Λ and may be represented in a form that differs from ΛCDM via a so-called deviation parameter b, such that at as $b \to 0$, $f(R) \to R - 2\Lambda$. These models also recover ΛCDM at high redshifts or, equivalently, large R. Using observations of type Ia Supernovae (SNe), baryonic acoustic oscillations, the cosmic microwave background, the Hubble parameter $H(z)$, and cosmic chronometers data, the free parameters in these models have been well constrained [21–23], and in some cases [24,25], the fits do not show any statistically significant difference from ΛCDM.

Among the plethora of cosmological data used to constrain these models, the angular-size redshift cosmological test has been used sparingly partly due to the lack of standard rulers, i.e., sources of which the intrinsic diameter is known, and the added complication arising from a possible size evolution with redshift. This test is based on the notion that, for all known models other than Milne [26–33], the angular diameter distance $d_A(z)$ attains a maximum value at some finite redshift $z_{\max}$. Among the various integrated distance (and temporal) measures used in cosmology, $d_A(z)$ uniquely has this property of reducing to zero approaching the big bang. This effect follows [34] from the fact that the angular diameter distance depends on the apparent angular size of the emitter. In this paper, we will be using the intrinsic size $\theta_{\rm core}$ of a compact quasar core, the value of which increases as we go back in time ($z \to \infty$), when the object was closer to us, so that $d_A(z) \sim \theta_{\rm core}^{-1}$ becomes smaller. Take the Einstein-de Sitter model ($\Omega = 1$) as an illustrative example. Its angular diameter distance $d_A^{\rm EdS}(z) = 2c/H_0(1+z)^{-1}(1 - 1/\sqrt{1+z})$ attains its maximum at $z_{\max} = 1.25$, while for flat ΛCDM with the *Planck* parameters [35] $\Omega_m = 1 - \Omega_\Lambda = 0.308$,

$$d_A^{\Lambda\rm CDM}(z) = \frac{c}{H_0}\frac{1}{1+z}\int_0^z \frac{dz'}{\sqrt{\Omega_m(1+z'^3)+\Omega_\Lambda}} \quad (1)$$

reaches a maximum at $z_{\max} = 1.596$.

The first such angular diameter-redshift tests for cosmological models were conducted using kiloparsec-scale radio sources and galaxies [36,37], but due to the lack of a reliable and well-defined standard ruler, these tests were not successful. This was followed by studies of double-lobed quasars [38] in the redshift range $1 \le z \le 2.7$, which showed that the apparent angular size for these objects remained almost unchanged with the angular diameter distance. Later on, it became apparent that ultracompact radio sources [39] that have a much smaller angular size in the milli–arc second range can be used as standard measuring rods, even more when considering that their age is insignificant compared to the age of the Universe, so that they are free from long-term evolutionary effects. Following the study of compact radio sources with the very large baseline interferometry in Ref. [39], there were a number of subsequent investigations involving these sources that led to some general cosmological constraints.

When using these compact radio sources, one is usually faced with the challenge of differentiating between systematic differences and proper cosmological variations. This arises due to the fact that these sources are often present in a mixed population of Active Galactic Nuclei that constitute quasars, BL Lacertae objects, Optically Violent Variable quasars, etc. This deficiency was recently rectified in Refs. [29–31], where a subsample of quasar cores with a tractable amount of scatter and almost free of evolutionary effects was identified. In their study, Cao *et al.* [30] focused their analysis of $d_A(z)$ on the optimization of the parameters in ΛCDM. This approach, however, is not suitable for a broader study and model selection involving a diverse set of (possibly non-nested) cosmologies, such as we have in this paper. Principally for this reason, a subsequent study involving their quasar sample was carried out recently by Melia [32] and Melia and Yennapureddy [33], who, instead of preassuming any particular cosmological models to infer d_A and its turning point $z_{\max}$, used Gaussian processes (GPs) to analyze these 120 sources spanning the redshift range $0 \le z \le 3$ in a completely model-independent way.

Since the goal of this paper is to use $z_{\max}$ as our primary probe, it will be helpful to better understand the improvements made with this diagnostic in recent years. Cao *et al.*'s [29–31] criteria for selecting a suitable subsample of quasars to measure the angular-diameter distance was a key step forward that greatly facilitates our work in this paper. But there are several areas of improvement that make our analysis even better. First, the use of GPs to reconstruct the angular-diameter distance as a function of redshift instead of relying on the parametrization in specific models cannot be overstated. As noted earlier, only an approach such as this can ensure that the inferred distance is a true reflection of the actual observations. In the end, none of the presumed models may be correct, in which case their adopted parametrization for d_A is overly restrictive. A GP reconstruction is completely free of such constraints for models, such as we have in this paper, that are not nested with ΛCDM. The GP approach to this work was facilitated by our recent publication [40], in which we introduced a new area minimization statistic appropriate for the use of GP reconstruction in model selection. This statistic was not available to Cao *et al.* at the time when they carried out their analysis.

Second, while Cao *et al.* [29–31] carried out their model optimization using the individual quasars in the sample, in our analysis, we first binned the 120 selected sources into 20 redshift intervals prior to the GP reconstruction. A quick inspection of their data and best-fit curves shows that many sources lie several σ's away from the theoretical curves. In other words, the reported errors appear to be too small to represent the actual scatter in the data. For this reason,

our approach used binning of the individual sources, with a population variance based on assumed Gaussian variation within each bin to more reliably estimate the error associated with each datum. Not surprisingly, our errors are larger than those reported for each individual source because they are a better reflection of the overall scatter in the data. So, the GP reconstruction we use for this paper is based on this binning rather than on the use of individual sources that, as mentioned, should yield results more in line with the observed scatter in the data.

Third, and equally important, Cao *et al.* [29–31] optimized the "standard ruler" $\ell_{\rm core}$ and the Hubble parameter H_0 separately, while our approach optimizes just one unknown that combines these two parameters. This is another crucial improvement because, to separate $\ell_{\rm core}$ from H_0, one must combine the angular-size data with other kinds of observation. For example, Cao *et al.* used $H(z)$ data based on cosmic chronometers and baryon acoustic oscillations (BAOs). Unfortunately, this biases the results because, as is well known, all but three BAO measurements are model dependent. They require the preassumption of a particular ΛCDM model in order to separate redshift-space distortions from the actual BAO peak position. Contrary to the claim made by Cao *et al.*, their determination of $\ell_{\rm core}$ is therefore not model independent. As explained in Refs. [32,33], however, one can use the angular-size data from compact quasar cores to test cosmologies without optimizing the values of $\ell_{\rm core}$ and H_0 separately, which entirely avoids the bias introduced with the adoption of BAO measurements. Without this step, one would not be able to test other models, such as $f(R)$ cosmologies.

Finally, it is necessary to understand why the turning point in $d_A(z)$, $z_{\rm max}$, is a better diagnostic for our models than the overall angular-diameter distance itself. For $z_{\rm max}$, one does not need to know H_0, so its measurement is a different kind of test than $d_A(z)$, which depends on the Hubble constant. The complication with the latter is that H_0 is model dependent, so, unfortunately, one must identify both $\ell_{\rm core}$ and H_0 to use $d_A(z)$. The outcome of this difference is that the added flexibility of adjusting d_A by optimizing H_0 is not available for the comparison of $z_{\rm max}$, which makes the latter more robust and a better discriminator of different cosmological models.

Melia and Yennapureddy [33] determined that the angular-diameter distance attains a turning point at $z_{\rm max} = 1.70 \pm 0.20$. Since no cosmology was preassumed with this measurement, its inferred value serves as a new, independent probe of the geometry of the Universe. In their study, Melia and Yennapureddy demonstrated that a comparison of the predicted value of $z_{\rm max}$ with this measurement can differentiate one model from another quite well. Using this comparison with the predictions of various cosmologies in GR, they found that the most strongly favored is the $R_{\rm h} = ct$ universe [41–45], followed by *Planck* ΛCDM. At the same time, several others—notably Milne, which predicts no turning point at all—are ruled out at a very high level of significance, well beyond the nominal 3σ.

In this paper, we advance the use of this novel cosmological test in very significant ways. We obtain the predicted value of $z_{\rm max}$ for the four well-studied viable $f(R)$ models described above and see how this changes as a function of the deviation parameter b. For the values of the parameters in these models, we adopt the constraints obtained by Nunes *et al.* [22] using two different data sets. The first data set includes the recently released cosmic chronometers (CC) data and the locally measured Hubble parameter H_0, and the second set adds to these the type Ia SNe joint light curves (JLA) and BAO distance measurements. From the predicted values of $z_{\rm max}$, we identify those $f(R)$ models that are consistent with the measured value of $z_{\rm max}$.

The paper is organized as follows. In the next section, we introduce $f(R)$ theory and write down the field equations for a spatially flat Friedmann-Robertson-Walker (FRW) metric as a dynamical system involving dimensionless variables. Then, in Sec. III, we consider each $f(R)$ model and numerically solve the system of equations to obtain the angular-diameter distance $d_A(z)$ and the redshift $z_{\rm max}$ at which it attains its maximum value. We discuss how well the models account for the data and present our conclusion in Sec. IV. Unless otherwise noted, we use units such that $8\pi G = c = 1$.

II. $f(R)$ GRAVITY

In $f(R)$ theory, the Einstein-Hilbert action is modified by replacing the Ricci scalar R in the gravitational Lagrangian by an *a priori* arbitrary nonlinear function $f(R)$ such that the action becomes

$$S = \frac{1}{2}\int \mathrm{d}^4x\sqrt{-g}f(R) + S^{(m)}, \tag{2}$$

where $S^{(m)}$ is the matter contribution. Varying the action above with respect to the (inverse) metric tensor g^{ab} yields the following field equations,

$$f'(R)R_{ab} - \frac{f(R)}{2}g_{ab} = \nabla_a\nabla_b f'(R) - g_{ab}\Box f'(R) + T_{ab}, \tag{3}$$

where a prime denotes differentiation with respect to R, $\Box \equiv g^{ab}\nabla_a\nabla_b$, and T_{ab} is the energy momentum tensor corresponding to the matter part of the action $S^{(m)}$. Taking the trace of these equations gives

$$\Box R = \frac{1}{3f''(R)}[T - 3f'''(R)(\nabla R)^2 + 2f(R) - Rf'(R)], \tag{4}$$

with $T \equiv \rho - 3p$ being the trace of T_{ab}, where ρ and p are, respectively, the energy density and pressure of the matter distribution. Using (4) in (3), the field equations take the Einstein form

$$G_{ab} = \frac{1}{f'(R)}(T_{ab} + T^{\rm eff}_{ab}), \tag{5}$$

where

$$T^{\rm eff}_{ab} = \left[\frac{f(R) - Rf'(R)}{2} g_{ab} + \nabla_a\nabla_b f'(R) - g_{ab}\Box f'(R)\right] \tag{6}$$

is the energy momentum tensor of the so-called curvature fluid representing the higher order curvature corrections in the action. From the Einstein form of the field equations in (5), one can define the effective gravitational coupling to be $G_{\rm eff} \equiv G/f'(R)$. Also using (5), it is straightforward to show that the conservation of the total energy momentum implies that the energy momentum tensor for the matter distribution T_{ab} is independently conserved, i.e., $\nabla_a T^{ab} = 0$.

It is well known [46] that $f(R)$ theory can actually be considered as a scalar tensor theory, in the sense that it can be expressed as Brans-Dicke (BD) theory [47] with $\omega = 0$ and a nonzero scalar potential $V(\phi)$. This would seem to invalidate the theory because, when $\omega = 0$, the post-Newtonian parameter (PPN) $\gamma_{BD} = \frac{1+\omega}{2+\omega} = 1/2$ does not agree with $\gamma \sim 1$ required by Solar System tests. However standard BD-theory has a vanishing scalar potential, and the PPN parameter for $f(R)$ theory is given by a more complicated expression than that of the BD theory [48], allowing it to agree with the Solar System tests. For a general $f(R)$, the scalar field and associated potential are given by

$$\begin{aligned} \phi &\equiv f'(R), \\ V(\phi) &\equiv R(\phi)f'(R) - f(R[\phi]). \end{aligned} \tag{7}$$

Then, it is easy to show that Eqs. (3) and (4) reduce to the field equations of BD theory with $\omega = 0$ and a nontrivial potential $V(\phi)$ with $dV/d\phi = R$. In order to obtain the scalar potential $V(\phi)$, the equation $\phi = f'(R)$ needs to be invertible, and conversely, a given BD theory having $\omega = 0$ can be expressed as an $f(R)$ theory provided that the equation $dV(\phi)/d\phi = R$ is invertible.

The general spatially flat FRW metric is given by

$$ds^2 = -dt^2 + a(t)^2[dr^2 + r^2(d\theta^2 + \sin\theta^2 d\phi^2)], \tag{8}$$

where $a(t)$ is the normalized scale factor expressed in terms of the cosmic time, such that at the present time $t = t_0$, $a(t_0) = 1$. For this metric, the field equations (5) yield the Friedmann equations

$$3H^2 = \frac{1}{f'}\left[\rho + \frac{Rf' - f}{2} - 3Hf''\dot{R}\right], \tag{9}$$

and

$$2\dot{H} + 3H^2 = -\frac{1}{f'}\left[p + f'''\dot{R}^2 + 2H\dot{R}f'' + \ddot{R}f'' + \frac{f - Rf'}{2}\right], \tag{10}$$

where the overdot indicates a derivative with respect to cosmic time t. Moreover, the Ricci scalar can be expressed in terms of the Hubble parameter $H = \dot{a}/a$ by

$$R = 6(2H^2 + \dot{H}). \tag{11}$$

In addition, conservation of the energy momentum for the matter distribution leads to

$$\dot{\rho} = -3H(\rho + p). \tag{12}$$

It should be noted that any $f(R)$ cosmological model must satisfy a number of conditions related to its stability and the prediction of a matter-dominated era (see Refs. [15,16] for details), namely:

(i) $f'(R) > 0$ for $R \geq R_0 > 0$, where R_0 is the Ricci scalar at the present time for the FRW metric in (8). If the final attractor is de Sitter spacetime with Ricci scalar R_1, we also require that $f'(R) > 0$ for $R \geq R_1 > 0$.
(ii) $f''(R) > 0$ for $R \geq R_0 > 0$.
(iii) $f(R) \approx R - 2\Lambda$ for $R \gg R_0$, so that the model reduces to ΛCDM at early times.
(iv) $0 < (\frac{Rf''}{f'})(r) < 1$ at $r = -Rf'/f = -2$.

TABLE I. Best fit values for the free parameters b and Ω_m using CC + H_0 and JLA + BAO + CC + H_0 data sets, adopted from Ref. [22], and the corresponding value of $z_{\rm max}$ calculated in this paper and shown in Figs. 5 and 6.

Model	Parameters	CC + H_0	JLA + BAO + CC + H_0
	b	$0.107^{+0.316}_{-0.158}$	$0.048^{+0.062}_{-0.077}$
HS	Ω_m	$0.264^{+0.069}_{-0.058}$	$0.264^{+0.059}_{-0.055}$
	$z_{\rm max}$	$1.647^{+0.093}_{-0.081}$	$1.650^{+0.089}_{-0.072}$
	b	$0.229^{+0.254}_{-0.710}$	$0.111^{+0.070}_{-0.286}$
Starobinsky	Ω_m	$0.261^{+0.065}_{-0.055}$	$0.269^{+0.050}_{-0.042}$
	$z_{\rm max}$	$1.657^{+0.064}_{-0.080}$	$1.646^{+0.065}_{-0.062}$
	b	$0.425^{+0.400}_{-0.424}$	$0.196^{+0.124}_{-0.195}$
Tsujikawa	Ω_m	$0.261^{+0.063}_{-0.056}$	$0.284^{+0.041}_{-0.044}$
	$z_{\rm max}$	$1.657^{+0.095}_{-0.079}$	$1.625^{+0.063}_{-0.048}$
	b	$0.289^{+0.341}_{-0.289}$	$0.130^{+0.089}_{-0.130}$
Exponential	Ω_m	$0.261^{+0.064}_{-0.055}$	$0.284^{+0.040}_{-0.049}$
	$z_{\rm max}$	$1.668^{+0.102}_{-0.095}$	$1.640^{+0.090}_{-0.061}$

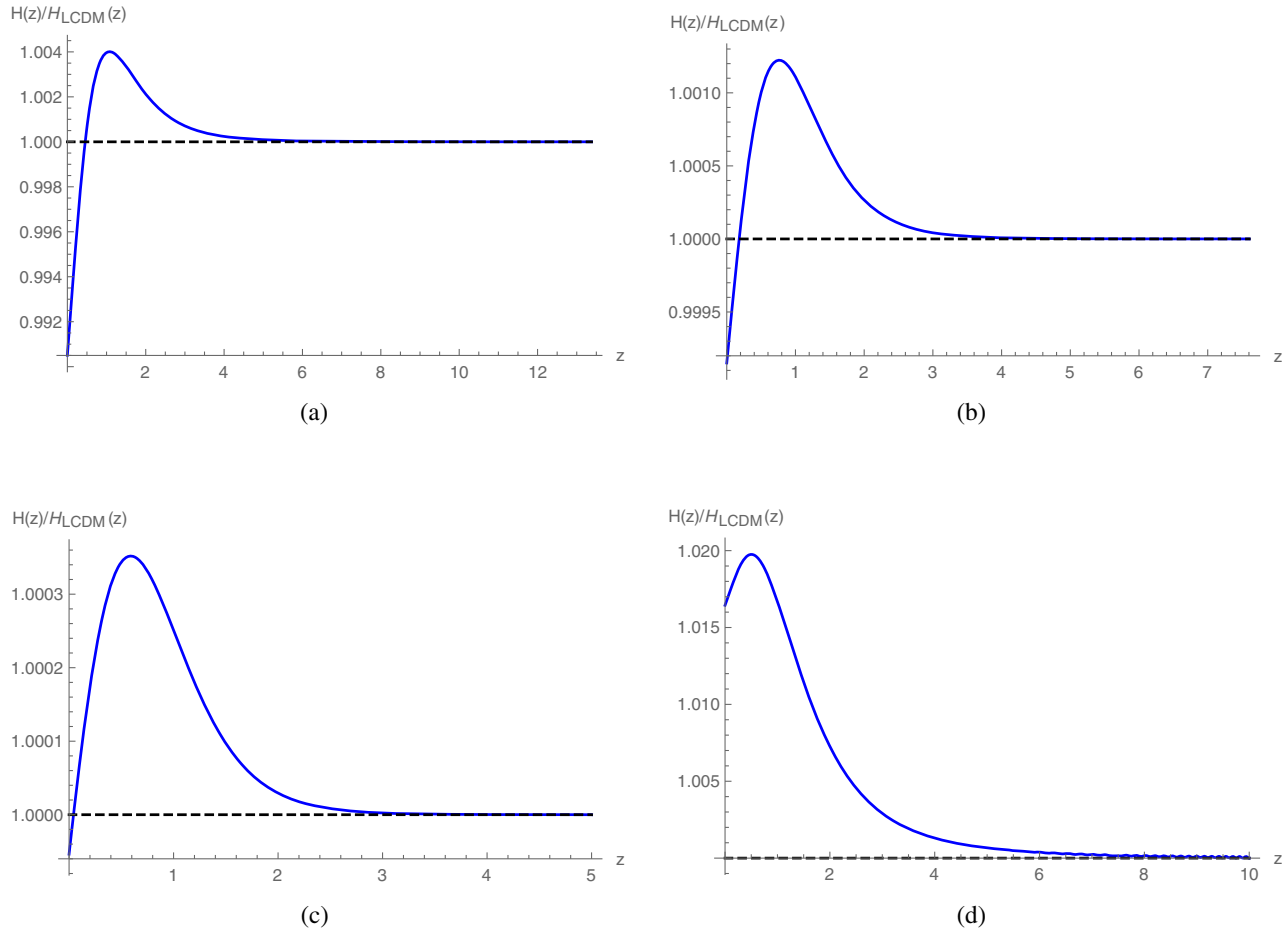

FIG. 1. Comparison of the Hubble parameter $H(z)$ with that in ΛCDM, $H^{\Lambda\mathrm{CDM}}(z)$, for (a) the HS model, (b) the Starobinsky model, (c) the Tsujikawa model, and (d) the exponential models. The best-fit values for the free parameters $\Omega_m^{\Lambda\mathrm{CDM}}$ and b used to obtain these plots are those derived from CC + H_0 data as given in Table I.

Instead of using cosmic time, we can also express the field equations in terms of the coordinate $x = \ln a = -\ln(1+z)$, such that at the present time $x(t_0) = 0$. In that case, Eqs. (11), (9), and (12) can be expressed as a dynamical system of the form [24]

$$\begin{aligned}\frac{dH}{dx} &= \frac{R}{6H} - 2H,\\ \frac{dR}{dx} &= \frac{1}{f''}\left(\frac{\rho}{3H^2} - f' + \frac{Rf' - f}{6H^2}\right),\\ \frac{d\rho}{dx} &= -3(\rho + p).\end{aligned} \tag{13}$$

The boundary conditions are obtained by requiring that, for large z (and large R), $f(R) \to R - 2\Lambda$, such that we recover the ΛCDM model, for which

$$\frac{H^2}{(H_0^{\Lambda\mathrm{CDM}})^2} = \Omega_m^{\Lambda\mathrm{CDM}}\exp(-3x) + \Omega_r^{\Lambda\mathrm{CDM}}\exp(-4x) + \Omega_\Lambda^{\Lambda\mathrm{CDM}}, \tag{14}$$

and

$$\frac{R}{2\Lambda} = 2 + \frac{\Omega_m^{\Lambda\mathrm{CDM}}}{2\Omega_\Lambda^{\Lambda\mathrm{CDM}}}\exp(-3x), \tag{15}$$

where $\Omega_\Lambda^{\Lambda\mathrm{CDM}} \equiv \Lambda/3(H_0^{\Lambda\mathrm{CDM}})^2$. The second equation is obtained by taking the trace of Einstein's field equations $R_{ab} - \frac{1}{2}g_{ab}R + \Lambda g_{ab} = T_{ab}$ and assuming that the matter and radiation components of the source are independently conserved. The quantities $\Omega_m^{\Lambda\mathrm{CDM}}$, $\Omega_r^{\Lambda\mathrm{CDM}}$, $\Omega_\Lambda^{\Lambda\mathrm{CDM}}$, and $H_0^{\Lambda\mathrm{CDM}}$ are the current values of the cosmological parameters and Hubble parameter, respectively, as calculated in ΛCDM. In general, these are different than the current corresponding parameters Ω_m^0, Ω_r^0, Ω_Λ^0 and Hubble parameter H_0 calculated in the $f(R)$ model. It is easy to show from the conservation equation for the source terms in (13), however, that

$$\Omega_m^{\Lambda\mathrm{CDM}}(H_0^{\Lambda\mathrm{CDM}})^2 = \Omega_m^0 H_0^2 = \frac{\rho_m(t_0)}{3} \tag{16}$$

and similarly for the radiation component.

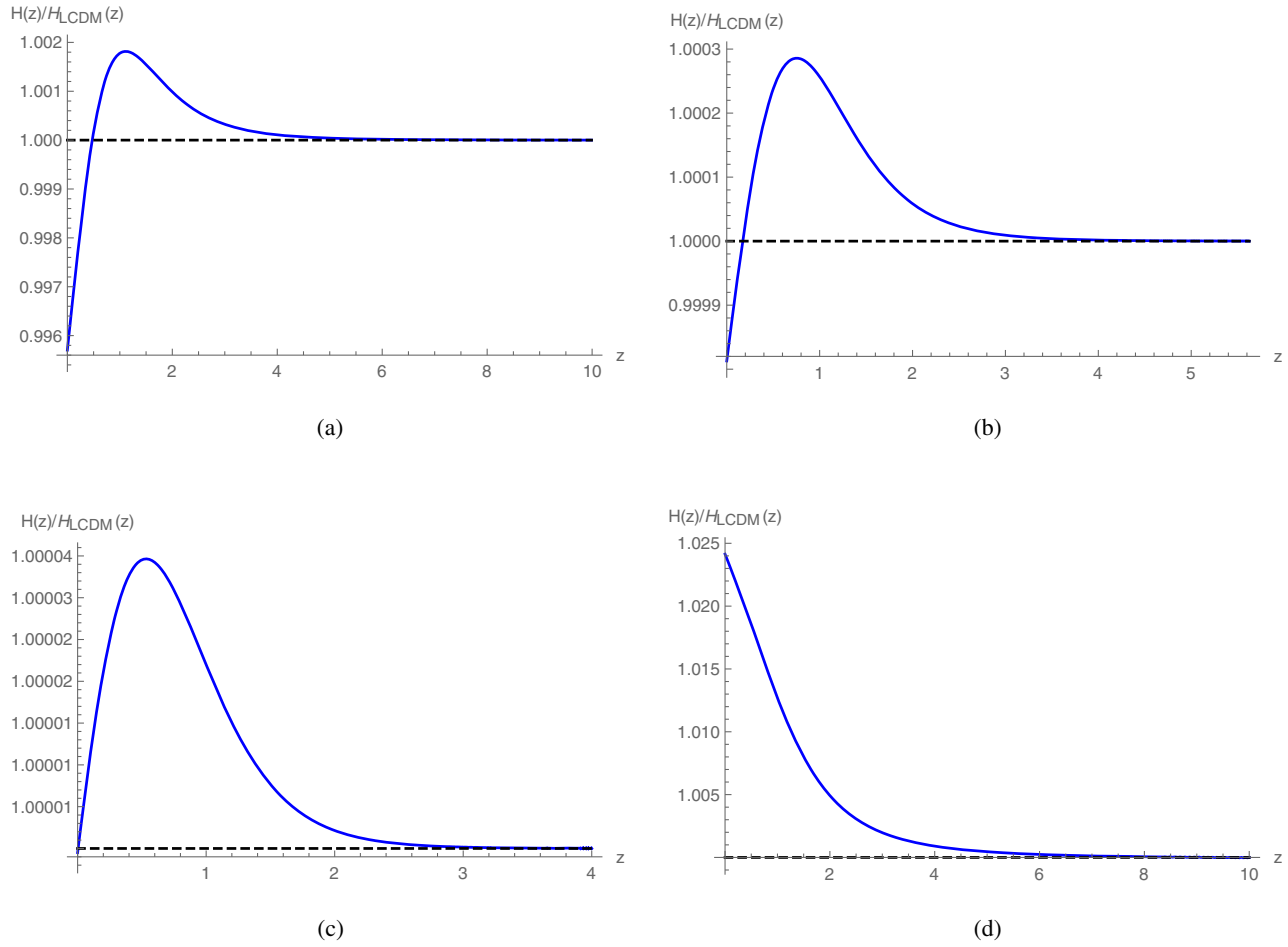

FIG. 2. Comparison of the Hubble parameter $H(z)$ with that in ΛCDM, $H^{\Lambda\mathrm{CDM}}(z)$, for (a) the HS model, (b) the Starobinsky model, (c) the Tsujikawa model, and (d) the exponential models. The best-fit values for the free parameters $\Omega_m^{\Lambda\mathrm{CDM}}$ and b used to obtain these plots are those derived from JLA + BAO + CC + H_0 data, as given in Table 1.

The field equations (13) can be written using the following dimensionless variables [24],

$$E \equiv \frac{H}{H_0^{\Lambda\mathrm{CDM}}}, \qquad \mathcal{R} \equiv \frac{R}{2\Lambda}, \tag{17}$$

in which case they take the form

$$\begin{aligned}\frac{dE}{dx} &= \Omega_\Lambda^{\Lambda\mathrm{CDM}}\frac{\mathcal{R}}{E} - 2E,\\ \frac{d\mathcal{R}}{dx} &= \frac{2\Lambda}{F_{\mathcal{R}\mathcal{R}}}\left[\frac{\Omega_m^{\Lambda\mathrm{CDM}}e^{-3x}}{E^2} + \frac{\Omega_r^{\Lambda\mathrm{CDM}}e^{-4x}}{E^2} - \frac{F_\mathcal{R}}{2\Lambda}\right.\\ &\quad \left. + \frac{(\mathcal{R}F_\mathcal{R} - F)\Omega_\Lambda^{\Lambda\mathrm{CDM}}}{2\Lambda E^2}\right],\end{aligned} \tag{18}$$

where $F_\mathcal{R} \equiv \frac{dF}{d\mathcal{R}}$ and $F_{\mathcal{R}\mathcal{R}} \equiv \frac{d^2F}{d\mathcal{R}^2}$. The boundary conditions are given by

$$\begin{aligned}E^2(x_i) &= \Omega_m^{\Lambda\mathrm{CDM}}e^{-3x_i} + \Omega_r^{\Lambda\mathrm{CDM}}e^{-4x_i} + \Omega_\Lambda^{\Lambda\mathrm{CDM}},\\ \mathcal{R}(x_i) &= 2 + \frac{\Omega_m^{\Lambda\mathrm{CDM}}e^{-3x_i}}{2\Omega_\Lambda^{\Lambda\mathrm{CDM}}},\end{aligned} \tag{19}$$

where the position $x_i = \ln a_i = -\ln(z_i + 1)$ is chosen such that the model approaches ΛCDM. After solving the dynamical system in (18) using the above boundary conditions, one can obtain the angular diameter distance

$$d_A(z) = \frac{1}{1+z}\int_0^z \frac{dz'}{H(z')} = e^x \int_x^0 \frac{e^{-x'}}{H(x')}dx', \tag{20}$$

the turning point of which may be evaluated in order to find the redshift $z_{\max}$.

III. COSMOLOGICAL MODELS

In this section, we consider some of the more popular, viable $f(R)$ models, for which we solve the system of equations in (18), and then calculate the redshift $z_{\max}$ and its dependence on the deviation parameter b:

(i) The Hu-Sawicki (HS) model [16] is given by $f(R) = R - m^2\frac{c_1(R/m^2)^n}{1+c_2(R/m^2)^n}$, where c_1 and c_2 are free parameters and m and n are positive constants, with $m^2 \approx \Omega_m^0 H_0^2$ being of the order of the Ricci scalar R_0

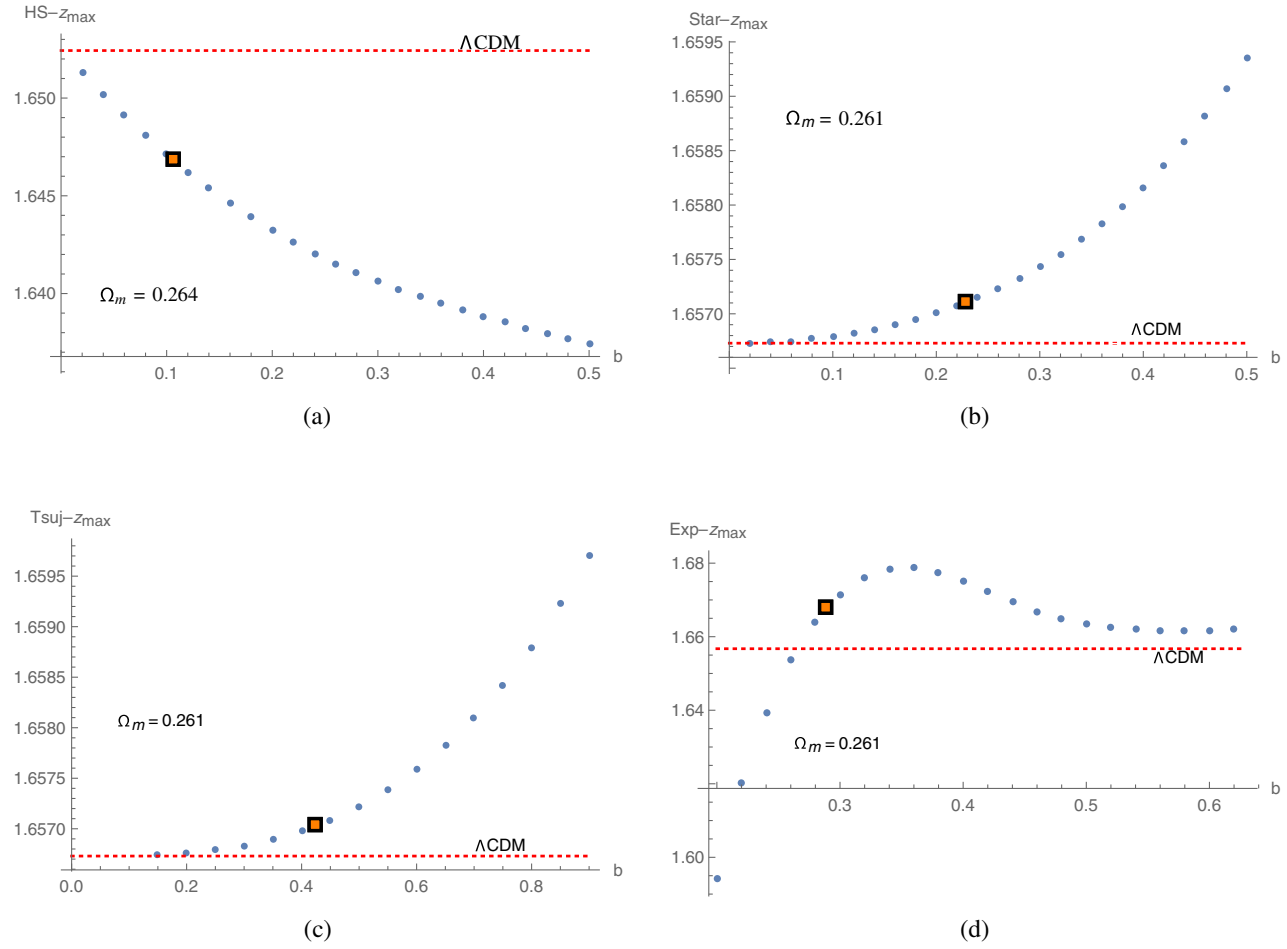

FIG. 3. Dependence of the predicted redshift z_{max} on the deviation parameter b for (a) the HS model, (b) the Starobinsky model, (c) the Tsujikawa model, and (d) the exponential model using the CC + H_0 data as shown in Table I. The range of values of b for each model corresponds to the uncertainty in its constrained value as discussed in the text. The constrained value of b itself and its associated z_{max} are shown by a filled box. The value of the free parameter Ω_m for each case is included in each subfigure. The red dotted line marks the value of z_{max} for ΛCDM ($b = 0$) assuming the same cosmological parameters as in the $f(R)$ model and is obtained from Eq. (21).

at the present time. This can be expressed in the ΛCDM form [20] $f(R) = R - 2\Lambda(1 - \frac{1}{1+(R/b\Lambda)^n})$, with $\Lambda = c_1 m^2/2c_2$ and $b = 2c_2^{1-1/n}/c_1$. In our case, we consider the case $n = 1$, the conventional approach seen in the literature.

(ii) In the Starobinsky model [17], $f(R) = R - c_1 m^2[1 - (1 + R^2/m^4)^{-n}]$, where c_1 is a free parameter and m and n are positive constants, with $m^2 \approx \Omega_m^0 H_0^2$ as in the HS case. This can also be expressed as a perturbation of ΛCDM [20], with $f(R) = R - 2\Lambda(1 - \frac{1}{(1+[\frac{R}{b\Lambda}]^2)^n})$, where $\Lambda = c_1 m^2/2$ and $b = 2/c_1$. Again, we take $n = 1$.

(iii) The Tsujikawa model was proposed in Ref. [18] and is given by $f(R) = R - \lambda R_c \tanh(\frac{R}{R_c})$, where λ and R_c are positive constants. It was shown [49] that the stability condition mentioned earlier requires that $\lambda > 0.905$. It was also shown [50] that this constraint for λ satisfies the Solar System and binary pulsar tests as well. For $R \gg R_c$, the model behaves like the exponential model with $f(R) \approx R - \lambda R_c(1 - \exp[-2R/R_c])$. The model can be expressed in the form $f(R) = R - 2\Lambda \tanh(\frac{R}{b\Lambda})$, where the deviation parameter $b = 2/\lambda < 2.21$.

(iv) The exponential model was first proposed independently by Cognola *et al.* [13] and Linder [19], and this model may be expressed in the form [24] $f(R) = R - 2\Lambda(1 - \exp[-\frac{R}{b\Lambda}])$, where $b > 0$ is the deviation parameter, such that it reduces to ΛCDM when $b \to 0$.

The table above shows the best-fit constrained values of the free parameters b and Ω_m (together with the corresponding 1σ errors) for each $f(R)$ model using the two separate data sets, namely $CC + H_0$ and JLA + BAO + CC + H_0 as obtained in Ref. [22], as well as the calculated values of z_{max} and their corresponding errors shown in Figs. 5 and 6. By solving the system of equations (18) for each $f(R)$ model using the constrained values shown in

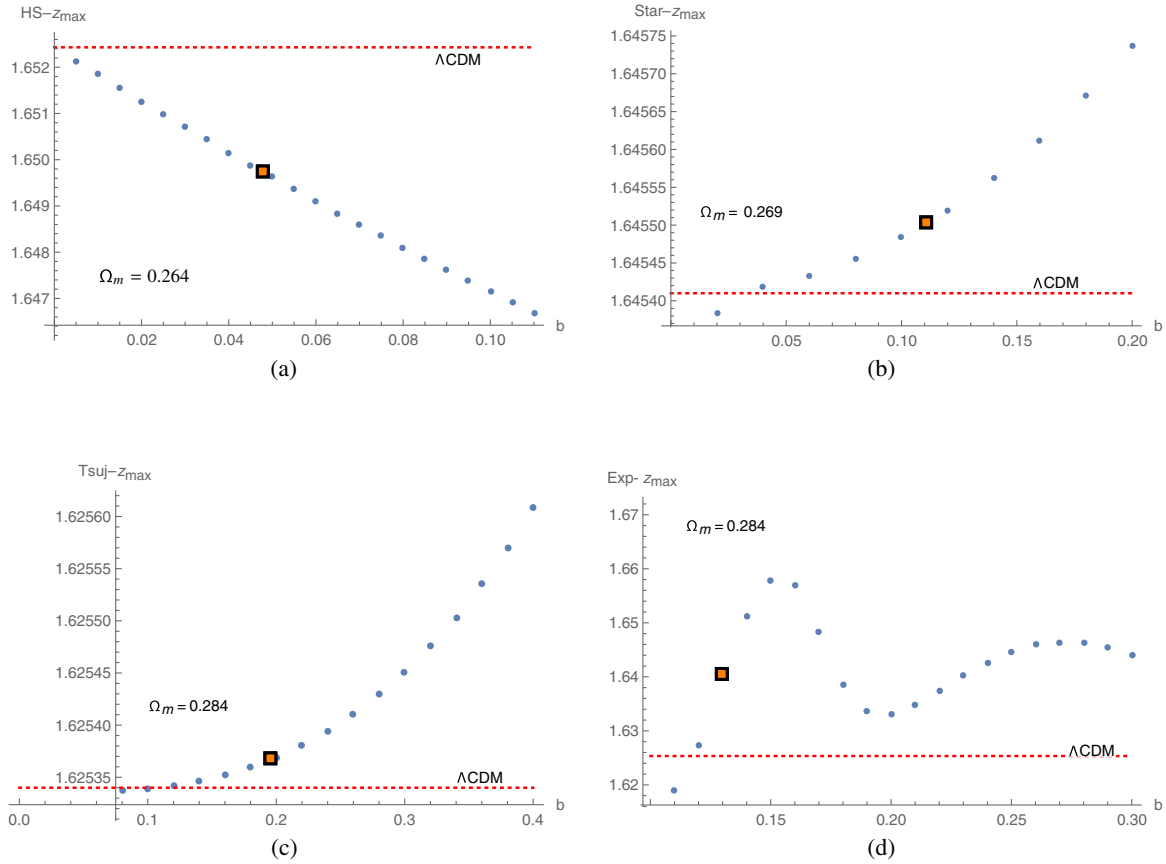

FIG. 4. Dependence of the predicted redshift $z_{\max}$ on the deviation parameter b for (a) the HS model, (b) the Starobinsky model, (c) the Tsujikawa model, and (d) the exponential model using the JLA + BAO + CC + H_0 data as shown in Table I. The range of values of b for each model corresponds to the uncertainty in its constrained value as discussed in the text. The constrained value of b itself and its associated $z_{\max}$ are shown by a filled box. The value of the free parameter Ω_m for each case is included in each subfigure. The red dotted line marks the value of $z_{\max}$ for ΛCDM ($b = 0$) assuming the same cosmological parameters as in the $f(R)$ model and is obtained from Eq. (21).

Table I, we obtain numerically the Hubble parameter $H(z)$ that is compared with the corresponding value $H_{\Lambda\mathrm{CDM}}$ for the ΛCDM model. This is shown for both data sets in Figs. 1 and 2 above. As expected, all of the models deviate from ΛCDM at small z (i.e., $z < 2$–3). It is also observed that when the combined data set JLA + BAO + CC + H_0 is used, the constrained value of the deviation parameter b takes a smaller value and therefore, as seen from Figs. 1 and 2, the difference between the $f(R)$ model and ΛCDM is smaller.

After numerically solving the system of equations in (18), we then calculate the angular diameter distance $d_A(z)$ for each model using Eq. (20), and from this, we obtain the redshift $z_{\max}$ at which $d_A(z)$ attains its maximum value. Figures 3 and 4 show the dependence of $z_{\max}$ on the deviation parameter b for each model using the CC + H_0 and JLA + BAO + CC + H_0 data sets, respectively. In each case, the fixed value of Ω_m corresponds to its constrained value, as listed in Table I. The range of values for b in each plot covers the uncertainty in b, as shown in Table I. The filled box represents the position of $z_{\max}$ for the constrained values of the parameters b and Ω_m. Figures 5 and 6 show the dependence of $z_{\max}$ on Ω_m, for the fixed constrained values of b. Again in this case, the range of values of Ω_m corresponds to the uncertainty in this parameter, as shown in Table I.

For each model, we also show (with a dotted red line in Figs. 3 and 4 and a dashed curve in Figs. 5 and 6) the redshift $z_{\max}$ for ΛCDM ($b = 0$) assuming the same cosmological parameters. For the ΛCDM, the angular diameter distance is given by (1). In this case, one can obtain (see, e.g., Eq. (10) in Ref. [51]) a closed form expression for $z_{\max}$ as a function of $\Omega_m^{\Lambda\mathrm{CDM}}$ in terms of elliptic integrals, as follows,

$$\frac{g}{\sqrt{1-\Omega_m^{\Lambda\mathrm{CDM}}}}\left[F(\phi,k)|_{(1+z)^{-1}=1}-F(\phi,k)|_{(1+z_{\max})^{-1}}\right] = \frac{1+z_{\max}}{\sqrt{\Omega_m^{\Lambda\mathrm{CDM}}(1+z_{\max})^3+(1-\Omega_m^{\Lambda\mathrm{CDM}})}}, \tag{21}$$

where

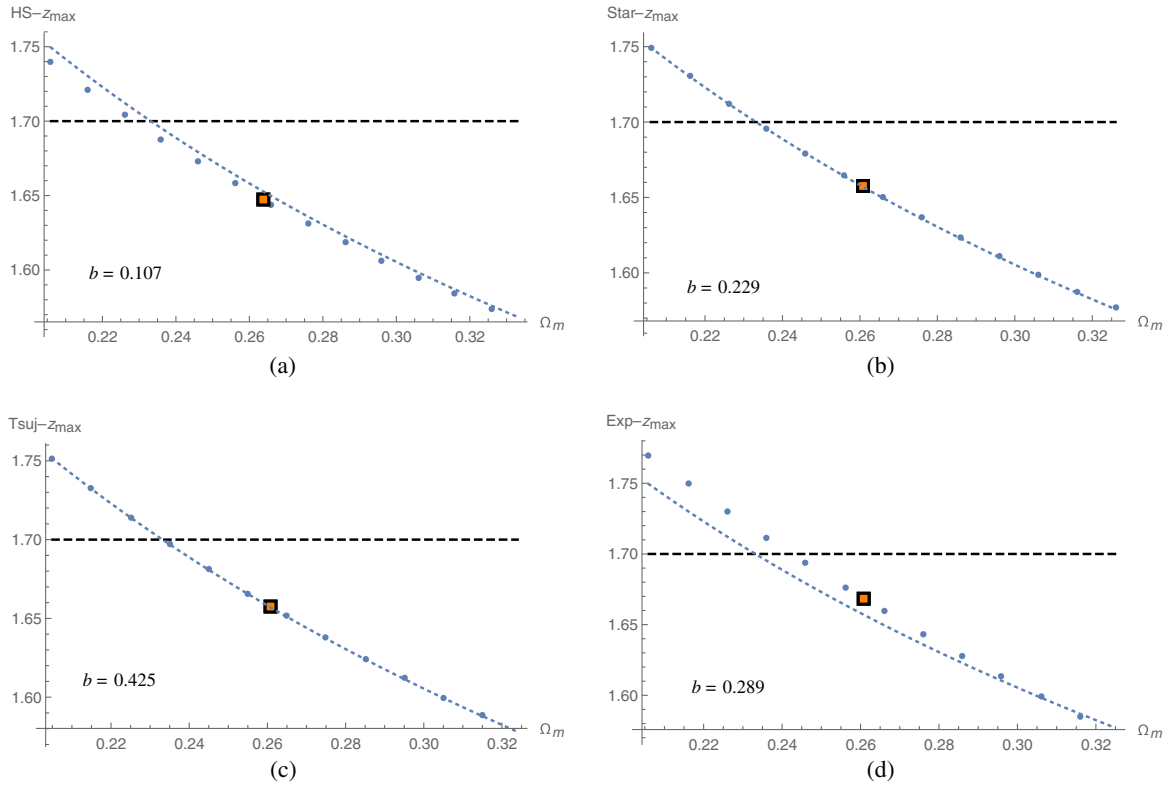

FIG. 5. Dependence of the predicted redshift $z_{\max}$ on the density parameter Ω_m for (a) the HS model, (b) the Starobinsky model, (c) the Tsujikawa model, and (d) the exponential model using the CC + H_0 data as shown in Table I. The range of values of Ω_m for each model corresponds to the uncertainty in its constrained value as discussed in the text. The constrained value of Ω_m itself and its associated $z_{\max}$ is shown by a filled box. The value of the deviation parameter b for each case is included in each subfigure. The dashed curve shows the behavior of $z_{\max}$ with Ω_m for ΛCDM ($b = 0$) obtained using Eq. (21). The black dashed line marks the observed value of $z_{\max}$.

$$\phi = \cos^{-1}\left[\frac{-m(1+z)+(\sqrt{3}-1)}{-m(1+z)-(\sqrt{3}+1)}\right],$$
$$m = \left[\frac{\Omega_m^{\Lambda\mathrm{CDM}}}{1-\Omega_m^{\Lambda\mathrm{CDM}}}\right]^{1/3},$$
$$k^2 = \frac{1}{2}+\frac{\sqrt{3}}{4},$$
$$g = \frac{1}{3^{1/4}}\left[\frac{1-\Omega_m^{\Lambda\mathrm{CDM}}}{\Omega_m^{\Lambda\mathrm{CDM}}}\right]^{1/3}. \quad (22)$$

The above expression represents the dotted curves in Figs. 5 and 6. In some cases, such as the Starobinsky and Tsujikawa models, the dependence of $z_{\max}$ on Ω_m is practically indistinguishable from that in ΛCDM, considering that the Hubble parameter $H(z)$ for these models is very similar to $H_{\Lambda\mathrm{CDM}}(z)$, even at low redshifts, as seen in Figs. 1 and 2. This happens even more when the whole JLA + BAO + CC + H_0 data set is used, due to the smaller magnitude of the constrained parameter b for each model. Moreover, the position of $z_{\max}$ in Figs. 3 and 4 approaches its ΛCDM value as $b \to 0$, as expected. For the exponential model, the system of equations (18) becomes stiff for the range of values of b shown in Table I, so to solve these equations, we have decided to use a Padé approximation to the exponential function. This is the reason why in this case $z_{\max}$ does not tend to the ΛCDM value as $b \to 0$.

In all the models we consider here, we find that the predicted value of $z_{\max}$ is consistent to within 1σ with the measured value 1.7 ± 0.2, throughout the previously constrained range of the deviation parameter b. We do find potentially interesting differences and trends, however, that one may hope to exploit with future, higher precision measurements of $z_{\max}$. For example, note that, while the Starobinsky and Tsujikawa models predict a redshift $z_{\max}$ that approaches the observed value as b increases, the opposite behavior is seen from the Hu-Sawicki model, where the predicted turning point $z_{\max}$ worsens with increasing deviation relative to that in ΛCDM. This remains valid for both data sets, as can be seen clearly in Figs. 3 and 4. Eventually, this test may provide a reliable measure of b, independently of all other previously employed methods, should the tension between the prediction of ΛCDM and the measured value of $z_{\max}$ persist as the precision of the observations continues to improve.

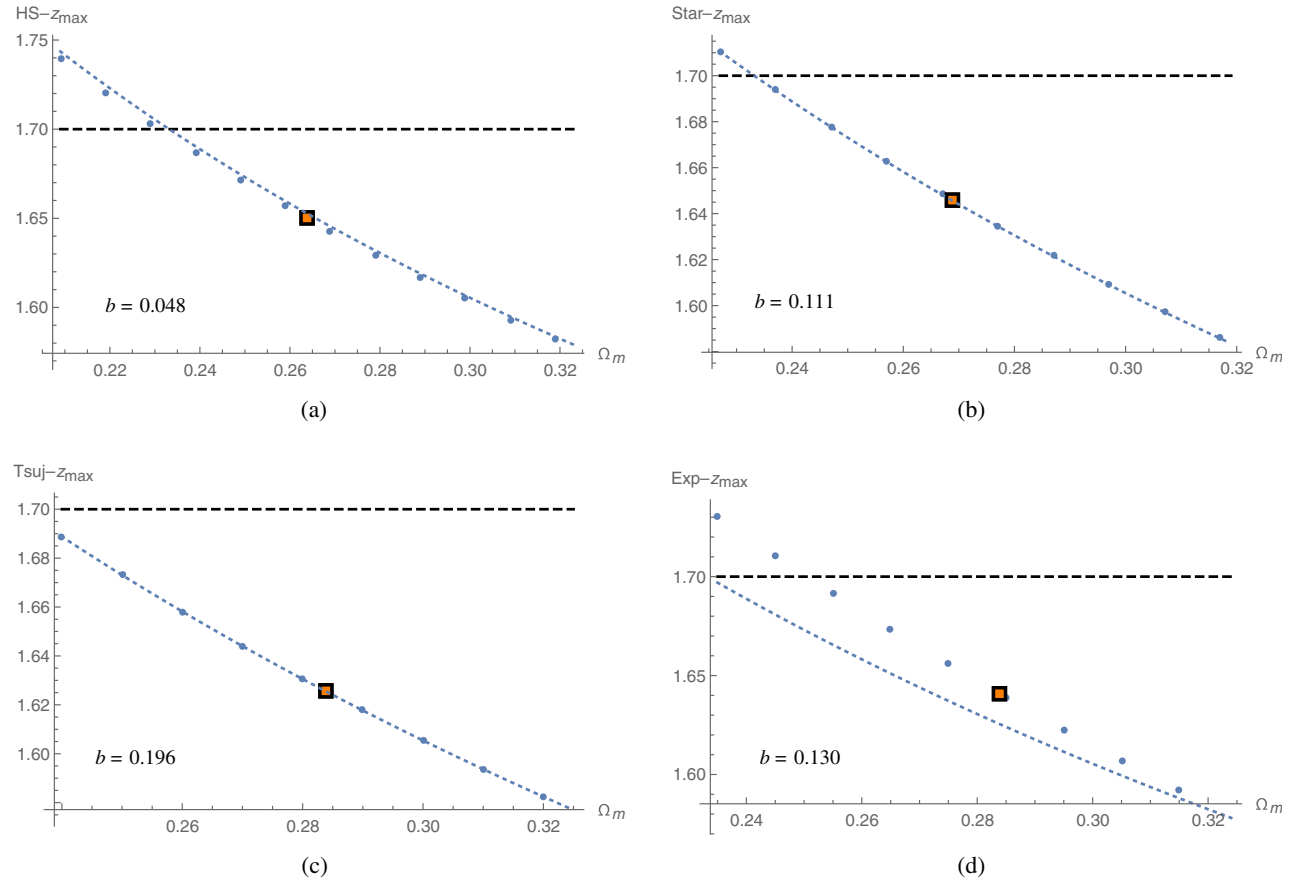

FIG. 6. Dependence of the predicted redshift $z_{\max}$ on the density parameter Ω_m for (a) the HS model, (b) the Starobinsky model, (c) the Tsujikawa model, and (d) the exponential model using the JLA + BAO + CC + H_0 data as shown in Table I. The range of values of Ω_m for each model corresponds to the uncertainty in its constrained value as discussed in the text. The constrained value of Ω_m itself and its associated $z_{\max}$ are shown by a filled box. The value of the deviation parameter b for each case is included in each subfigure. The dashed curve shows the behavior of $z_{\max}$ with Ω_m for ΛCDM ($b = 0$) obtained using Eq. (21). The black dashed line marks the observed value of $z_{\max}$.

IV. DISCUSSION AND CONCLUSION

In this paper, we have compared four currently popular and viable $f(R)$ cosmological models on the basis of their predicted turning point $z_{\max}$ in the angular diameter distance. This has been done by first numerically solving the coupled system (18) for $H(z)$ and then using this in the expression for the angular diameter distance in (20) to locate where it attains its maximum value for the constrained range of the deviation parameter b in each model. For these models, we have adopted the best-fit values of the free parameters obtained in Ref. [22], using cosmic chronometer data and the locally measured value of H_0, combined with the type Ia SN joint light curves and BAO distance measurements. We should point out the issue that the locally measured H_0 used by Nunes *et al.* [22] in their analysis is not consistent with the smoothed-out cosmological value in any cosmological model, including ΛCDM, where it is in tension with the *Planck* value by over 9%. The extent of this deviation between these values of H_0 for the $f(R)$ models presented here is not clear to us at this point. In addition, we should point out that the BAO distance measurements are generally made with the adoption of ΛCDM as the background cosmology in order to resolve the redshift-space distortions [52]. As such, the optimization of model parameters in Ref. [22] is at least partially model dependent.

Our comparison of the predicted $z_{\max}$ with its measured value must therefore be viewed with this caveat in mind. Nevertheless, we have seen that in most cases the redshift $z_{\max}$ of the turning point changes considerably, not only between a given $f(R)$ model and ΛCDM to which it converges but also between the $f(R)$ models themselves. The promise of differentiating between the various versions of $f(R)$ theories using the measurement of $z_{\max}$ with compact-quasar cores thus represents an entirely new probe of the geometry of the Universe, which goes beyond the reach of type Ia SNe. This diagnostic can be particularly useful in those cases where $f(R)$ models are almost indistinguishable [25] from ΛCDM when using other "conventional" cosmological data.

We point out, in particular, that the two most popular, viable $f(R)$ models in the literature, namely the Hu-Sawicki and Starobinsky models, predict quite a different behavior for $z_{\max}$ as a function of b, in spite of the fact that both models recover ΛCDM when $b \to 0$ and for large values of z and R. In the former case, $z_{\max}$ decreases with b, so it worsens the tension between ΛCDM and the data. Though the precision of this measurement is not yet sufficient for us to rule out either model in favor of the other, the early indication is that the angular-diameter distance test seems to slightly favor Starobinsky's theory over the Hu-Sawicki model. The other models indicate that the turning point redshift $z_{\max}$ approaches the measured value as the deviation parameter b increases, keeping their viability intact. Moreover, this observed behavior does not change when one takes into consideration the uncertainty in the best-fit values of the free parameter Ω_m.

For a next step, we plan to derive analytic expressions for the angular-diameter distance $d_A(z)$ in the various $f(R)$ models, to be used in rather obvious extensions to the work reported here. The promising outcome of our analysis warrants an optimizaton of the model parameters—particularly the deviation parameter b—utilizing a simultaneous fit to both the $d_A(z)$ and $H(z)$ data. While some debate still persists in the literature regarding whether or not one may legitimately merge measurements of $H(z)$ using different techniques, there appears to be a consensus growing that a determination of the Hubble parameter based solely on the use of cosmic chronometers may be made in a truly model-independent fashion [40,53–56]. With two sets of model-independent data available for this cross-correlation—the angular diameter distance to compact quasar cores and the differential time-redshift relationship dt/dz obtained from cosmic chronometers—there are therefore strong indications that a meaningful prioritization of the various $f(R)$ theories may emerge. The outcome of this work will be reported elsewhere.

[1] T. Clifton, P. G. Ferreira, A. Padilla, and C. Skordis, Phys. Rep. **513**, 1 (2012).
[2] V. Faraoni, *Cosmology in Scalar-Tensor Gravity* (Kluwer Academic, Dordrecht, Netherlands, 2004).
[3] T. P. Sotiriou and V. Faraoni, Rev. Mod. Phys. **82**, 451 (2010).
[4] I. Neupane and B. M. N. Carter, J. Cosmol. Astropart. Phys. 06 (2006) 004.
[5] T. Koivisto and D. F. Mota, Phys. Lett. B **644**, 104 (2007).
[6] S. Vacaru, Int. J. Mod. Phys. D **21**, 1250072 (2012).
[7] P. D. Mannheim, Prog. Part. Nucl. Phys. **56**, 340 (2006).
[8] A. A. Starobinsky, Phys. Lett. **91B**, 99 (1980).
[9] S. M. Carroll, V. Duvvuri, M. Trodden, and M. S. Turner, Phys. Rev. D **70**, 043528 (2004).
[10] A. D. Dolgov and M. Kawasaki, Phys. Lett. B **573**, 1 (2003).
[11] S. Nojiri and S. D. Odintsov, Phys. Rev. D **68**, 123512 (2003).
[12] T. Chiba, Phys. Lett. B **575**, 1 (2003).
[13] G. Cognola, E. Elizalde, S. Nojiri, S. D. Odintsov, L. Sebastiani, and S. Zerbini, Phys. Rev. D **77**, 046009 (2008).
[14] L. Amendola, D. Polarski, and S. Tsujikawa, Phys. Rev. Lett. **98**, 131302 (2007).
[15] L. Amendola, R. Gannouji, D. Polarski, and S. Tsujikawa, Phys. Rev. D **75**, 083504 (2007).
[16] W. Hu and I. Sawicki, Phys. Rev. D **76**, 064004 (2007).
[17] A. A. Starobinsky, JETP Lett. **86**, 157 (2007).
[18] S. Tsujikawa, Phys. Rev. D **77**, 023507 (2008).
[19] E. V. Linder, Phys. Rev. D **80**, 123528 (2009).
[20] K. Bamba, A. Lopez-Revelles, R. Myrzakulov, S. D. Odintsov, and L. Sebastiani, Classical Quantum Gravity **30**, 015008 (2013).
[21] S. Basilakos, S. Nesseris, and L. Perivolaropoulos, Phys. Rev. D **87**, 123529 (2013).
[22] R. C. Nunes, S. Pan, E. N. Saridakis, and E. M. C. Abreu, J. Cosmol. Astropart. Phys. 01 (**2017**) 005.
[23] J. Pérez-Romero and S. Nesseris, Phys. Rev. D **97**, 023525 (2018).
[24] S. D. Odintsov, D. Gómez Sáez-Chillón, and G. S. Sharov, Eur. Phys. J. C **77**, 862 (2017).
[25] A. De la Cruz-Dombriz, P. K. S. Dunsby, K. Sulona, and D. Sáez-Gómez, Phys. Rev. D **93**, 084016 (2016).
[26] W. H. McCrea, Z. Astrophys. **9**, 290 (1935).
[27] F. Hoyle, Evidence for Gravitational Theories, in *Proceedings of Enrico Fermi School of Physics, Course XX, Varenna*, edited by C. Moller (Academic, New York, 1961), p. 141.
[28] G. F. R. Ellis and G. Tivon, The Observatory **105**, 189 (1985).
[29] S. Cao, M. Biesiada, X. Zheng, and Z.-H. Zhu, Astrophys. J. **806**, 66 (2015).
[30] S. Cao, M. Biesiada, J. Jackson, X. Zheng, Y. Zhao, and Z.-H. Zhu, J. Cosmol. Astropart. Phys. 02 (2017) 012.
[31] S. Cao *et al.*, Astron. & Astrophys. **606**, A15 (2017).
[32] F. Melia, Europhys. Lett. **123**, 39001 (2018).
[33] F. Melia and M. K. Yennapureddy, Mon. Not. R. Astron. Soc. **480**, 2144 (2018).
[34] F. Melia, Classical Quantum Gravity **30**, 155007 (2013).
[35] P. A. R. Ade *et al.* (Planck Collaboration), Astron. & Astrophys. **594**, A13 (2016).
[36] K. P. Kapahi, Observational Cosmology, in *Proceedings of IAU Symposium, Beijing, People's Republic of China, 1986*, edited by A. Hewitt, G. Burbidge, and L. Z. Fang (D. Reidel Publishing Co., Dordrecht, Netherlands, 1987), pp. 251–265.
[37] K. Nilsson, M. J. Valtonen, J. Kotilainen, and T. Jaakkola, Astrophys. J. **413**, 453 (1993).

[38] A. Buchalter, D. J. Helfand, R. H. Becker, and R. L. White, Astrophys. J. **494**, 503 (1998).
[39] L. I. Gurvits, K. I, Kellermann, and S. Frey, Astron. Astrophys. **342**, 378 (1999).
[40] F. Melia and M. K. Yennapureddy, J. Cosmol. Astropart. Phys. 02 (2018) 034.
[41] F. Melia, Mon. Not. R. Astron. Soc. **382**, 1917 (2007).
[42] F. Melia and M. Abdelqader, Int. J. Mod. Phys. D **18**, 1889 (2009).
[43] F. Melia and A. S. H. Shevchuk, Mon. Not. R. Astron. Soc. **419**, 2579 (2012).
[44] F. Melia, Front. Phys. **11**, 119801 (2016).
[45] F. Melia, Am. J. Phys. **86**, 585 (2018).
[46] V. Faraoni, Accelerated Cosmic Expansion, in *Proceedings of the Fourth International Meeting on Gravitation and Cosmology*, edited by C. M. Gonzales, J. E. M. Aguilar, and L. M. R Barrera, Astrophysics and Space Science Proceedings (Springer, New York, 2014), Vol. 38, pp. 19–32.
[47] C. Brans and R. H. Dicke, Phys. Rev. **124**, 925 (1961).
[48] S. Capozziello, A. Stabile, and A. Troisi, Phys. Lett. B **686**, 79 (2010).
[49] A. De Felice and S. Tsujikawa, Living Rev. Relativity **13**, 3 (2010).
[50] T. Liu, X. Zhang, and W. Zhao, Phys. Lett. B **777**, 286 (2018).
[51] M. E. Araújo and W. R. Stoeger, Mon. Not. R. Astron. Soc. **394**, 438 (2009).
[52] F. Melia and M. López-Corredoira, Int. J. Mod. Phys. D **26**, 1750055 (2017).
[53] F. Melia and R. S. Maier, Mon. Not. R. Astron. Soc. **432**, 2669 (2013).
[54] F. Melia and T. M. McClintock, Astron. J. **150**, 119 (2015).
[55] J.-J. Wei, F. Melia, and X. Wu, Astrophys. J. **835**, 270 (2017).
[56] K. Leaf and F. Melia, Mon. Not. R. Astron. Soc. **470**, 2320 (2017).